Fingerprints of changes in annual and seasonal precipitation from CMIP5 models over land and ocean

Fingerprints of Changes in Annual and Seasonal Precipitation from CMIP5 Models over Land and Ocean

Beena Balan Sarojini[1,2], Peter Stott[3], Emily Black[1,2], and Debbie Polson[4]

[1]National Centre for Atmospheric Science - Climate Division, Reading, UK

[2]Walker Institute, University of Reading, Reading, UK

[3]Met Office Hadley Centre, Exeter, UK

[4]University of Edinburgh, Edinburgh, United Kingdom

28 September 2012

(Revised version to GRL)

Corresponding author: Beena Balan Sarojini (b.balansarojini@reading.ac.uk)

NCAS - Climate, Department of Meteorology

University of Reading, Reading RG6 6BB, United Kingdom

Phone: + 44 118 378 6238, Fax: + 44 118 378 8316

Abstract

By comparing annual and seasonal changes in precipitation over land and ocean since 1950 simulated by the CMIP5 (Coupled Model Intercomparison Project, phase 5) climate models in which natural and anthropogenic forcings have been included, we find that clear global-scale and regional-scale changes due to human influence are expected to have occurred over both land and ocean. These include moistening over northern high latitude land and ocean throughout all seasons and over the northern subtropical oceans during boreal winter. However we show that this signal of human influence is less distinct when considered over the relatively small area of land for which there are adequate observations to make assessments of multi-decadal scale trends. These results imply that extensive and significant changes in precipitation over the land and ocean may have already happened, even though, inadequacies in observations in some parts of the world make it difficult to identify conclusively such a human fingerprint on the global water cycle. In some regions and seasons, due to aliasing of different kinds of variability as a result of sub sampling by the sparse and changing observational coverage, observed trends appear to have been increased, underscoring the difficulties of interpreting the apparent magnitude of observed changes in precipitation.

Key words: Precipitation, Global climate models, Observations, Anthropogenic climate change, Detection and attribution

Index terms: 1600 Global Change, 1626 Global climate models (3337, 4928), 3354 Precipitation (1854), 1655 Water cycles (1836), 1635 Oceans (1616, 3305, 4215, 4513), 1637 Regional climate change (4321)

1. Introduction

Over the last 50 years, increased surface temperatures have been observed over many parts of the globe (Sánchez-lugo et al., 2012; Morice et al., 2012), a trend that has been attributed to anthropogenic forcing (Hegerl et al., 2007; Stott et al., 2010). From a theoretical standpoint, it is expected that higher temperatures will be accompanied by an amplification of the hydrological cycle (Boer, 1993; Allen and Ingram, 2002; Held and Soden, 2006; Solomon et al., 2007). Expected changes are observed in many variables of the hydrological cycle (Huntington, 2006; Bates et al., 2008; Allan and Liepert, 2010) such as an increase in surface specific humidity (Willett et al., 2007) and a decrease in ocean salinity (Durack and Wijffels, 2010). Precipitation is the most easily observed component of the hydrological cycle and for this reason has been the focus of most analyses of hydrological change. However, precipitation is influenced by both local thermodynamic factors (for example a warmer ocean) (Hoerling et al., 2012; Liu et al., 2012) and remote circulation patterns (for example ENSO) (Santer et al., 2009) – and is thus noisy and highly variable. Nevertheless, several studies have detected anthropogenic changes in the hydrological cycle. Using CMIP3 multi-model data, changes in zonal mean annual land precipitation for a single observational dataset have been attributed to anthropogenic forcing (Zhang et al., 2007) and zonal mean seasonal land changes for three different observational datasets have been attributed to external forcing, for all seasons other than June, July and August (JJA) (Noake et al., 2012). Using the CMIP5 models and allowing for differences in observational data coverage, an anthropogenic signal has been detected for changes in zonal mean seasonal land precipitation for four different observational datasets for March, April and May (MAM); but detection was dataset dependent for other seasons (Polson et al., 2012). On a regional scale, an anthropogenic signal has been identified

for the northern high latitudes (Min et al., 2008) and also within some latitudinal bands (Noake et al., 2012; Polson et al., 2012).

It is clear from Polson et al., (2012) as well as from other recently published work (e.g. Arkin et al., (2011)) that the biases in observational data that arise from incomplete spatial and temporal coverage may obscure the true trends. Comparing model data at locations where observations are available, with model data everywhere provides a means of exploring this limitation. This study, for the first time carries out such an analysis - utilizing the CMIP5 multi-model data in conjunction with the extended Zhang station-based gridded dataset (Zhang et al., 2007).

Previous studies of the cause of changes in the hydrological cycle have moreover considered only changes in precipitation on land where long time series of observed station data are available. Although changes in land precipitation have the clearer socio-economic impact, changes in oceanic precipitation affect the continental scale processes that drive the hydrological cycle (Trenberth, 2011). The shortness of the period for which satellite data are available, however, precludes formal detection and attribution studies for oceanic regions. Nevertheless, analysis of model data can provide useful information about the origin of changes in the hydrological cycle, even in regions for which long time series of observations are currently unavailable. Understanding of the expected fingerprints of change can help guide where observational dataset developments, including use of satellite data (Huffman et al., 2007), need to be focused. This study therefore builds on previous attribution studies by examining where human induced changes in both oceanic and land precipitation on annual and seasonal time scales are expected to have already appeared.

2. Models and Data

2.1 Coupled Model Simulations

We use the climate model output of simulations of the historical period (1850-2005) available from the CMIP5 data archive (Table S1). The data were extracted from a suite of integrations designed for detecting and attributing anthropogenic climate change signals. The experiments we analysed were forced with i) both anthropogenic and natural forcings (ALL) and ii) only natural forcings (NAT). Specifically, the ALL experiments were forced with observed anthropogenic forcings of greenhouse gases, tropospheric aerosols, ozone and natural forcings of solar variations and volcanic aerosols, and the NAT experiments were forced only with natural solar variations and aerosols from major volcanic eruptions. Comparison between ALL and NAT runs can be used to distinguish anthropogenic and natural climate changes.

2.2 Observational Data

The dataset chosen is an extended version of the monthly precipitation observations used in Zhang et al., (2007), which is based on station data extracted from the Global Historical Climatology Network (GHCN) (Vose et al., 1992). The data are from 1901-2009, gridded at 5X5^{o}, quality-controlled, and provided for all land grid squares on the globe for which station data are available.

3. Methodology

In order to assess recent (1951-2005) changes in precipitation, both in the model world and the real world, we calculated annual and seasonal precipitation anomalies with respect to the baseline climatology of 1961-90 (Figure 1a), where the observational data are available for greater than 90% of the total time period. This additional quality control criterion was applied to the Zhang data in order to avoid artefacts arising from significant changes in data coverage during the study. The

effect of the exclusion of grid cells because of the quality control measures described above is evident in Figure 1b, which shows the observed spatial trends.

Further details of the model simulations, observational data and methods by which the data were masked to the observational grid are given in the Supplementary Information (Table S1, Text S1).

4. Results

We compare the global and zonal scale changes in annual and seasonal precipitation in observations and as simulated by the CMIP5 models using anthropogenic and natural forcings. In the observations, there is no clear trend in precipitation globally for either annual or seasonal time series (Figures S1-S5, first row). This is perhaps not surprising and is in agreement to earlier studies (Zhang et al., 2007). It is clear from Figure 1b that the observed trend in northern hemisphere precipitation varies spatially – both in sign and magnitude. There is an upward trend in precipitation throughout the high latitudes (Min et al., 2008) whereas in the tropics, there is considerable variation (Zhang et al., 2007). Much of Africa, for example has experienced a decrease in precipitation, while there has been an increase in Central and South America and relatively little change in India. This is consistent with time series of observed precipitation from 1951-2005, which show that during December, January and February (DJF) and JJA, in the northern high latitudes, observed precipitation has increased (Figure S6c, S6d) and that elsewhere trends are weak and inconsistent (Figures S2 and S4, last column).

Within the climate models, when all points are considered, the data are less noisy than when the data are masked by the observational coverage. Comparison between the ALL and NAT simulations for annual global time series in the unmasked model data (Figure 2a, 2b and 2c) shows that the difference between the ALL and NAT multi-

model means increases towards the end of the time series. In other words, an anthropogenic influence on global-scale precipitation is statistically significant, in model data, by the 1990s, when all grid points are included in the analysis. When the model data is masked by the land observational coverage (hereafter masked land), although an upward trend is evident, there is significant difference between the ALL and NAT integrations only by yr 2000 (Figure 2d). The global response of volcanic aerosols from major eruptions (Gillett et al., 2004) is evident in both the ALL and NAT runs - with decreased precipitation due to the effect of Pinatubo (1992) and Agung (1964) more pronounced than that of El Chichon (1983).

Looking at zonal scales, a significant anthropogenic signal of increase in annual precipitation appears in the models over the northern high latitudes of 60^{o}N-90^{o}N both over land, ocean and masked land, by the 1990s, in the ALL runs and an increase is also seen in the observations (Figure S1 second row, Figure 1b). On seasonal scales, it is interesting to note that, during DJF, a significant anthropogenic signal is seen both over northern high latitude land and ocean (Figure 3a, 3b), and over the northern subtropical oceans (Figure 3c, 3d), by the 2000s. This significant northern high latitude moistening is evident over land, oceans, and masked land and observations during all the seasons (Figures S2-S5, second row) indicating the robustness of the signal. Our results are consistent with previous findings of an anthropogenic increase in precipitation over northern high latitude land areas detected using the CMIP3 models and observations (Min et al., 2008).

On masked land, both models and observations show greater interannual variations within the zonal seasonal time series than within the global seasonal time series. Figure S6 shows an example of this during DJF and JJA. Despite these short-term variations, the long-term Arctic moistening signal seen in the models is also

consistent with observed changes in this region. Dai et al., (2009) reported an increase in freshwater discharge from the Arctic land regions in to the Arctic Ocean. They show a positive trend in discharge towards the end of the 20th century. Although surface warming plays a primary role in increased discharge from ice and frost covered higher latitude land areas, the observed increase in precipitation (Figure 1b) may also have contributed to the increase in discharge.

In the tropical (30^{o}S-30^{o}N) and southern subtropical bands (60^{o}S-30^{o}S), there is no clear signal of change due to anthropogenic forcing on either annual or seasonal timescales (Figures S1-S5, fourth and fifth rows) and also the models show less agreement with each other over the land areas in these two bands. The increase in annual precipitation in the tropics in both ALL and NAT runs, towards the end of the time series, seems to be related to changing observational coverage causing larger anomalies to be represented in the zonal means of model simulations in recent years. Seasonally, these increases are seen in JJA which persist through September, October and November (SON). In the southern higher latitudes (90^{o}S-60^{o}S), modelled changes show significant increase in precipitation predominantly contributed by the ocean part, which is present throughout the seasons (Figures S1-S5, last row). The significant change occurs by the 1990s for annual, austral spring and summer, and by the 2000s for austral autumn. No significant differences between the ALL and NAT multi-model means are found over land and ocean in the 30^{o}S-30^{o}N band, annually and seasonally, except for increased precipitation over ocean in the boreal winter, by the 2000s.

Although it is more difficult to detect a separation between the masked NAT and ALL runs, in most seasons and zonal bands, the trends in the full model data are seen to some degree in the masked data. In some cases (global annual and in SON, 30^{o}N-

60^{o}N annual and in DJF and SON), moreover, the masked data apparently have a stronger trend than in the unmasked data – suggesting that the observed global or zonal mean trends may be aliased due to sub sampling by sparsity of data coverage.

We confirm that the simulated precipitation changes between ALL and NAT runs are indeed due to the difference in anthropogenic and natural climate forcings, and not due to the difference in the unequal number of ALL and NAT simulations of different models. For instance, for annual time series, ALL and NAT multi-model means of identical GCMs (Figure S8) show similar differences as the same when all available ALL and NAT runs (Figure S1) are considered.

5. Summary and Discussion

On global and annual scales, a significant, albeit small, signal of human influence in precipitation can be identified within climate models over both land and ocean. On zonal and seasonal scales, a robust signal of increase in precipitation due to anthropogenic forcings is found over the northern high latitudes within both land and ocean. The strength of the trend in anthropogenically forced precipitation in the northern high latitudes is consistent with the existing evidence of human influence on the Arctic (Min et al., 2008).

Within the oceans, we find that the northern high latitude moistening during boreal winter is accompanied by moistening over the northern subtropical oceans (no significant change is seen for northern subtropical land). We also find that the ocean in southern higher latitudes receives increased precipitation – consistent with an observed freshening of polar oceans (Durack and Wijffels, 2010). This increase in precipitation is seen only when anthropogenic forcings are considered, suggesting that the precipitation and hence the salinity trend has an anthropogenic origin. In relation

to amplification of other variables of the hydrological cycle by humans, regionally, our results of increased precipitation over the Arctic are in agreement with previous findings of observed increase in continental discharge (Dai et al., 2009) and ocean freshening (Durack and Wijffels, 2010); and, globally, increased precipitation over land and ocean is consistent with observed increase in surface specific humidity over land and ocean (Willett et al., 2007).

When the model data are masked by land observational coverage, trends in precipitation are, in some cases obscured. Moreover, comparison of simulated changes over land (with all grid points) to that over land masked by observational coverage and to observed changes reveal large excursions in the time series, notably in the southern zonal bands where data is spatially limited. The sparse and infrequent observations are not showing the true magnitude and variability in global or zonal mean precipitation. Furthermore, although the increased noise makes it difficult to isolate an anthropogenic influence, trends in model data masked by observational coverage are, in some cases greater than trends in the unmasked data (i.e. at all points on the globe with no allowance made for observational coverage) globally and in certain zonal bands. It could be partly due to the fact that the observational coverage of the dataset used in this study is spatially limited compared to other gridded datasets with greater coverage owing to spatial interpolation of data to grid points where station data are not available. Care must therefore be taken when interpreting trends in global or regional precipitation taking into account data availability, as aliasing of one type of variability at a location on to another type of variability at a different location as a result of sub sampling of data (Von Storch and Zwiers, 2004) due to sparse data coverage may result in an apparent increase (or decrease) of inferred trends in

precipitation. Using multiple observational datasets may help to overcome some of these issues.

In summary, we find that the latest generation of climate models in CMIP5 show that precipitation is expected to have increased globally and that there is a significant anthropogenic component to these changes in the model output. The strongest trends are seen in the northern high latitudes, during the boreal winter – with weaker trends evident in the zonal mean subtropics and tropics. We also find significant anthropogenic increases are expected to have occurred in ocean precipitation – suggesting that the observed changes in salinity reported in previous studies have an anthropogenic origin.

Acknowledgements

This work is supported by PAGODA project of the Changing Water Cycle programme of UK Natural Environment Research Council (NERC) under grant NE/I006672/1 and by the Joint DECC/Defra Met Office Hadley Centre Climate Programme (GA01101). We acknowledge the CMIP5 climate modelling groups, for producing and making their model output available, the U.S. Department of Energy's Program for Climate Model Diagnosis and Intercomparison (PCMDI) which provides co-ordinating support for this data and led development of software infrastructure in partnership with the Global Organization for Earth System Science Portals for CMIP and the World Climate Research Programme's Working Group on Coupled Modelling (WGCM), which is responsible for CMIP. We thank Xuebin Zhang for providing the observational data.

References

Allan, R. P., and B. G. Liepert (2010), Anticipated changes in the global atmospheric water cycle, *Environ. Res. Lett. 5* 025201, doi:10.1088/1748-9326/5/2/025201.

Allen, M., and W. Ingram, (2002), Constraints on future changes in climate and the hydrologic cycle, *Nature, 419*, 224-232, doi 10.1038/nature01092.

Arkin, P. A., T. M. Smith, M. R. P. Sapiano, and J. Janowiak (2010), The observed sensitivity of the global hydrological cycle to changes in surface temperature, *Environ. Res. Lett. 5*, 035201, doi:10.1088/1748-9326/5/3/035201.

Bates, B. C., Z. W. Kundzewicz, S. Wu and J. P. Palutikof, Eds., (2008), Climate Change and Water, *Technical Paper of the Intergovernmental Panel on Climate* Change, IPCC Secretariat, Geneva, 210 pp.

Boer, G. J. (1993), Climate change and the regulation of the surface moisture and energy budgets, *Clim. Dynamics*, 8, 225-239.

Dai, A., T. Qian, K. E. Trenberth, and J. D. Milliman, (2009), Changes in continental freshwater discharge from 1948 to 2004, *J. Climate*, 22, 2773–2792, doi 10.1175/2008JCLI2592.1

Durack, P., and S. Wijffels, (2010), Fifty-year trends in global ocean salinities and their relationship to broad-scale warming, *Journal of Climate*, 4342-4362, doi 10.1175/2010JCLI3377.1.

Gillett, N., A. Weaver, F. Zwiers, and M. Wehner, (2004), Detection of volcanic influence on global precipitation, *Geophys. Res. Lett.*, ARTN L12217, doi 10.1029/2004GL020044.

Hegerl, G., T. Crowley, W. Hyde, M. Allen, H. Pollack, J. Smerdon, and E. Zorita (2007), Detection of human influence on a new, validated 1500-year temperature reconstruction, *J. Clim., 20*, 650–666.

Held, I., and B. Soden (2006), Robust responses of the hydrological cycle to global warming, *J. Clim., 19* (21), 5686–5699.

Hoerling, M., J. Eischeid, J. Perlwitz, X. Quan, T. Zhang, and P. Pegion (2012), On the increased frequency of mediterranean drought, *J. Clim., 25*, 2146–2161, doi 10.1175/JCLI-D-11-00296.1.

Huffman, G. J., R. F. Adler, D. T. Bolvin, G. Gu, E. J. Nelkin, K. P. Bowman, Y. Hong, E. F. Stocker, and D. B. Wolff (2007), The TRMM Multisatellite Precipitation Analysis (TMPA): quasi-global, multiyear, combined-sensor precipitation estimates at fine scales, *J. Hydrometeor, 8*, 38–55, doi: http://dx.doi.org/10.1175/JHM560.1.

Huntington, T. G. (2006), Evidence for intensification of the global water cycle: Review and synthesis, *Journal of Hydrology, 319*, 83-95.

Liu, C., R. P. Allan, and G. J. Huffman (2012), Co-variation of temperature and precipitation in CMIP5 models and satellite observations, *Geophys. Res. Lett., 39*, L13803, doi:10.1029/2012GL052093.

Min, S-K., X. Zhang, F. W. Zwiers (2008), Human-induced Arctic moistening, *Science 320*, 518-520.

Morice, C. P., J. J. Kennedy, N. A. Rayner, and P. D. Jones (2012), Quantifying uncertainties in global and regional temperature change using an ensemble of observational estimates: the HadCRUT4 dataset, *Journal of Geophysical Research* (accepted).

Noake, K., D. Polson, G. Hegerl, and X. Zhang (2012), Changes in seasonal land precipitation during the latter twentieth-century, *Geophys. Res. Lett., 39*, L03706, doi:10.1029/2011GL050405.

Polson, D., G. Hegerl, X. Zhang, and T. J. Osborne (2012), Causes of robust seasonal land precipitation changes, *J Climate* (submitted).

Sánchez-lugo, A., J. J. Kennedy, and P. Berrisford (2012), [Global climate] Surface temperature [in "State of the Climate in 2011"], *Bull. Amer. Meteor. Soc., 93 (7)*, S14–S15.

Santer, B. D., K. E. Taylor, P. J. Gleckler, C. Bonfils, T. P. Barnett, D. W. Pierce, T. M. L. Wigley, C. Mears, F. J. Wentz, W. Brueggemann, N. P. Gillett, S. A. Klein, S. Solomon, P. A. Stott, and M. F. Wehner (2009), Incorporating model quality information in climate change detection and attribution studies, *Proceedings of the National Academy of Sciences of the United States of America, 25 106*, 14778-14783.

Solomon, S., D. Qin, M. Manning, M. Marquis, K. Averyt, M. M. B. Tignor, H. L. Miller Jr., and Z. Chen, Eds. 2007: *Climate Change (2007), The Physical Science Basis, Contribution of Working Group I to the Fourth Assessment Report of the Intergovernmental Panel on Climate Change*. Cambridge: Cambridge University Press, 40-45.

Stott, P., N. Gillett, G. C. Hegerl, D. Karoly, D. Stone, X. Zhang, and F. Zwiers (2010), Detection and attribution of climate change: A regional perspective, *Wiley Interdiscip. Rev. Clim. Change, 1*, 192–211.

Trenberth, K. (2011), Attribution of climate variations and trends to human influences and natural variability, *Wiley Interdisciplinary Reviews: Climate Change, 2*, 925-930, doi: 10.1002/wcc.142.

Von Storch, H., and F. W. Zwiers (2004), Statistical analysis in climate research, Cambridge, U.K., Cambridge University Press, 513.

Vose, R., R. Schmoyer, P. Steurer, T. Peterson, R. Heim, T. Karl, and J. Eischeid (1992), The Global Historical Climatology Network: long-term monthly temperature, precipitation, sea level pressure, and station pressure data, *ORNL/CDIAC-53*, NDP-041.

Willett, K. M., P. D. Jones, N. P. Gillett, and P. W. Thorne (2007), Attribution of observed surface humidity changes to human influence, *Nature, 449*, 710–713, doi:10.1038/nature06207.

Zhang, X., F. W. Zwiers, G. C. Hegerl, F. H. Lambert, N. P. Gillett, P. A. Stott, and T. Nosawa (2007), Detection of human influence on twentieth-century precipitation trends, *Nature 448*, 461-466.

Auxiliary Material:

Table of coupled model simulations

Table S1: List of the CMIP5 Detection and Attribution (D&A) Models used in this study, their atmospheric and oceanic resolutions and the type of D&A experiments. ALL refers to experiments with both anthropogenic and natural forcings and NAT refers to experiments with natural forcings alone. Each realization (r1i1p1 for all models except for CCSM4 where r2i1p1 is used) of each model with an 'X' sign is used. More details of the set up of these D&A experiments can be found in Taylor et al., (2009).

Modelling Centre, Country	**Model Name**	**Atmosphere lon x lat x levels**	**Ocean lon x lat x levels**	**ALL**	**NAT**
MOHC, UK	**HadGEM2-ES**	1.875 x 1.25 x 38	1 x 1-0.3 x 40	X	X
CSIRO-QCCCE, Australia	**CSIRO-Mk3-6-0**	1.875 x 1.875 x 18	1.875 x 0.9375 x 31	X	X
NCC, Norway	**NorESM1-M**	2.5 x 1.875 x 26	1.125 x 0.5 x 53	X	X
CNRM-CERFACS, France	**CNRM-CM5**	1.4 x 1.4 x 31	1 x 1 x 42	X	X
CCCMA, Canada	**CanESM2**	2.8 x 2.8 x 35	1.4 x 0.94 x 40	X	X
BCC, China	**BCC-CSM1-1**	2.8 x 2.8 x 26	1 x 1-0.3 x 40	X	X
INM, Russia	**INMCM4_ESM**	2 x 1.5 x 21	1 x 0.5 x 40	X	
IPSL, France	**IPSL-CM5A-LR**	3.75 x 1.875 x 39	2 x 2 x 31	X	
NASA GISS, USA	**GISS-E2-H**	2.5 x 2 x 40	1.25 x 1 x 32	X	
NASA GISS, USA	**GISS-E2-R**	2.5 x 2 x 40	1.25 x 1 x 32	X	
MPI-M, Germany	**MPI-ESM-LR**	1.875 x1.875 x 47	~1.5 x ~1.5 x 40	X	
NOAA GFDL, USA	**GFDL-ESM2G**	2.5 x 2.0 x 24	1 x 0.9 x 50	X	
NOAA GFDL, USA	**GFDL-ESM2M**	2.5 x 2.0 x 24	1 x 0.85 x 63	X	
NCAR, USA	**CCSM4**	1.25 x 0.94 x 26	1.11 x 0.3-0.5 x 60	X	
MIROC, Japan	**MIROC5**	1.4 x 1.4 x 40	1.4 x 0.8 x 50	X	
MIROC, Japan	**MIROC-ESM**	2.8 x 2.8 x 80	1.4 x 0.94 x 44	X	X
MIROC, Japan	**MIROC-ESM-CHEM**	2.8 x 2.8 x 80	1.4 x 0.94 x 44	X	X
MRI, Japan	**MRI-CGCM3**	1.13 x 1.13 x 48	1 x 0.5 x 51	X	X
IPSL, France	**IPSL-CM5A-MR**	2.5 x 1.26 x 39	2 x 2 x 31	X	

Auxiliary Material: Text S1

Extended Methodology

Both annual and seasonal (DJF, MAM, JJA and SON) anomalies of precipitation were calculated for global data and the following zonal bands of 60^{o}N-90^{o}N, 30^{o}N-60^{o}N, 30^{o}S-30^{o}N, 60^{o}S-30^{o}S and 90^{o}S-60^{o}S. A baseline climatology of 1961-1990 was used for all anomaly calculations. Figure 1b shows the effect of the exclusion of grid cells because of the quality control measures (the 90% observational criterion) described in Section 3. In particular, the 30^{o}S-60^{o}S band, which has the least land points, has only about 7% of the global land observational coverage. In Antarctica (90^{o}S-60^{o}S band), none of the land grid points meets the quality control criteria applied in this study. A choice of observational data available for greater than 75% of the total time period increases the spatial coverage over South America, Africa, north east of Asia and Russia, however the sign of the observed trends in each zonal band is insensitive to the 75% observational criterion (Figure S7).

The data are masked to the observational grid in three stages. First, the simulated precipitation data available in different spatial resolutions (Table 1) are divided into land and ocean parts using their respective land-area fractions. Specifically, a point is chosen as land when its land-area fraction is greater than 70%. Sea ice is treated as an ocean point. Second, the data are interpolated to the $5X5^{o}$ Zhang data grid. Finally, the observational mask (with the 90% criterion) is applied to each regridded model data to obtain the consistent temporal and spatial data coverage for the simulated and observed data.

In both the observed and simulated cases, a 5-year running mean is applied to the resulting time series. For the precipitation changes discussed for the model world alone, all valid model grid points are considered - so the data are not masked by

observations. The division into land and ocean components and interpolation is carried out using the method described above.

The changes, discussed in Section 4, are tested for statistical significance using an independent two-sample two-tailed t-test for the last 30 years of the time series. When the changes are significant, the null hypothesis that the means simulated in ALL and NAT runs are the same is rejected with 95% confidence i.e. when the difference in means of ALL and NAT runs are significant at the 5% level. Trends in Figure 1b and Figure S7 are calculated as the slope of the linear regression of the time series at each spatial point.

Extended References

Taylor, K. E., R. J. Stouffer, G. A. Meehl, (2012), An overview of CMIP5 and the Experiment Design, Bull. Amer. Meteor. Soc., 93, 485-498, doi: 10.1175/BAMS-D-11-00094.1.

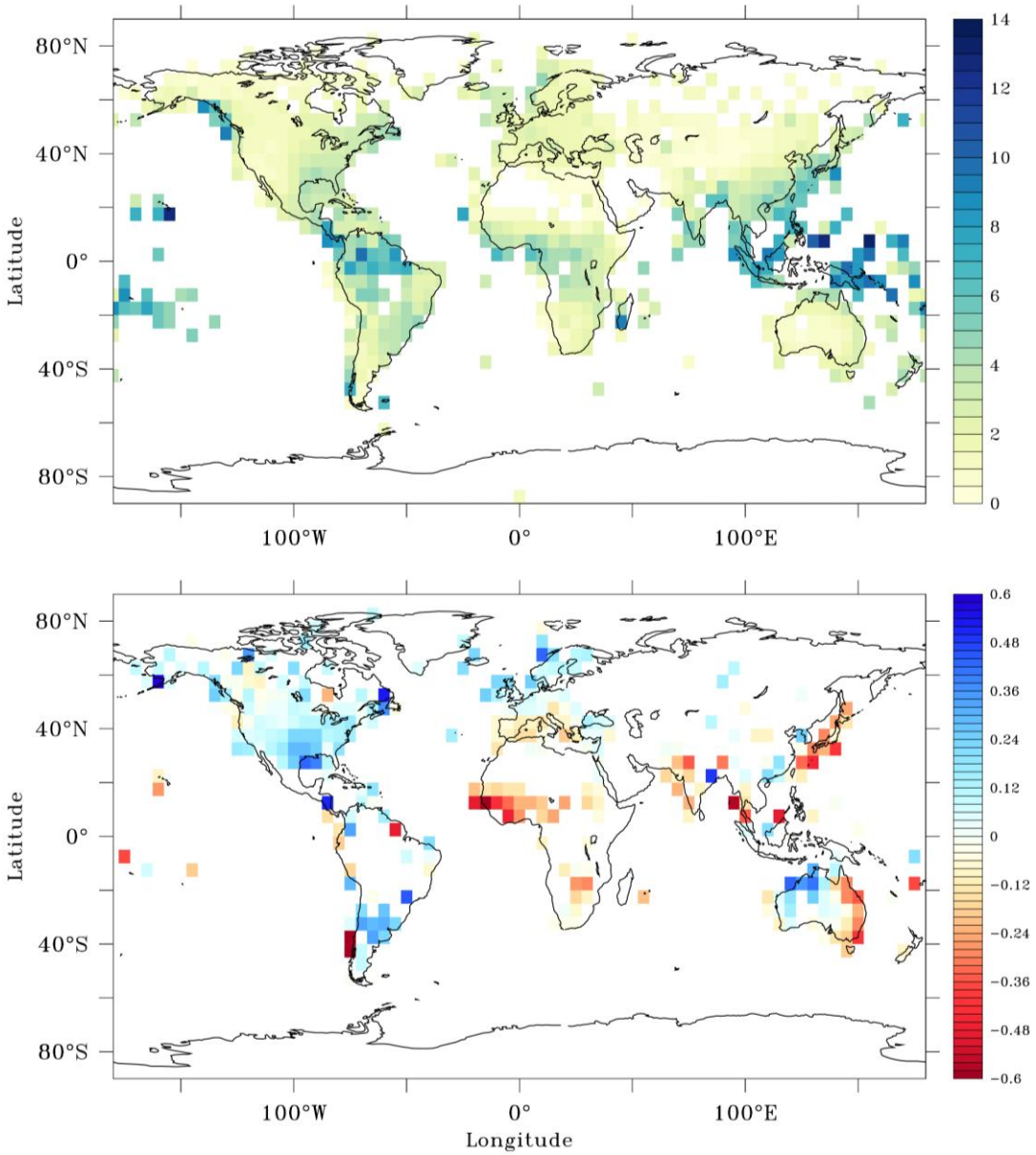

Figure 1: a) Observed climatological mean precipitation (mm/day) for the baseline period of 1961-90 (top). An updated version of Zhang et al., (2007) dataset is used. b) Spatial map of trend (mm/day/yr), for 1951-2005, which is the time period of the analysis (bottom). Positive trends (blue) and negative trends (red) are shown. Trends are calculated as the slope of the linear regression of the time series at each spatial point.

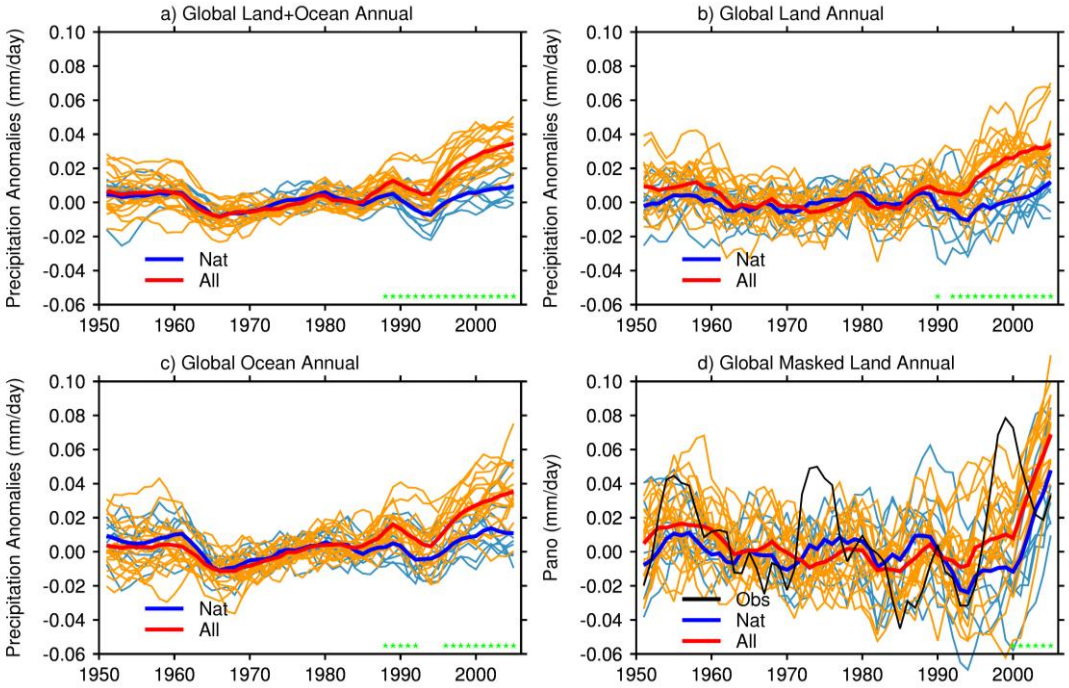

Figure 2: Global changes in annual precipitation (mm/day), expressed relative to the baseline period of 1961-90, simulated by CMIP5 models forced with, both anthropogenic and natural forcings (ALL) and natural forcings only (NAT). a) Land and Ocean, b) Land , c) Ocean, with all grid points, and d) Land masked by observational coverage. Blue lines show individual NAT simulations and red lines show individual ALL simulations specified in Table 1. Multi-model means are shown in thick solid lines and observations are in black solid line. A 5-yr running mean is applied to both simulations and observations. Green stars show statistically significant changes at 5% level (p value < 0.05) between ALL and NAT runs using a two-sample two-tailed t-test for the last 30 years of the time series.

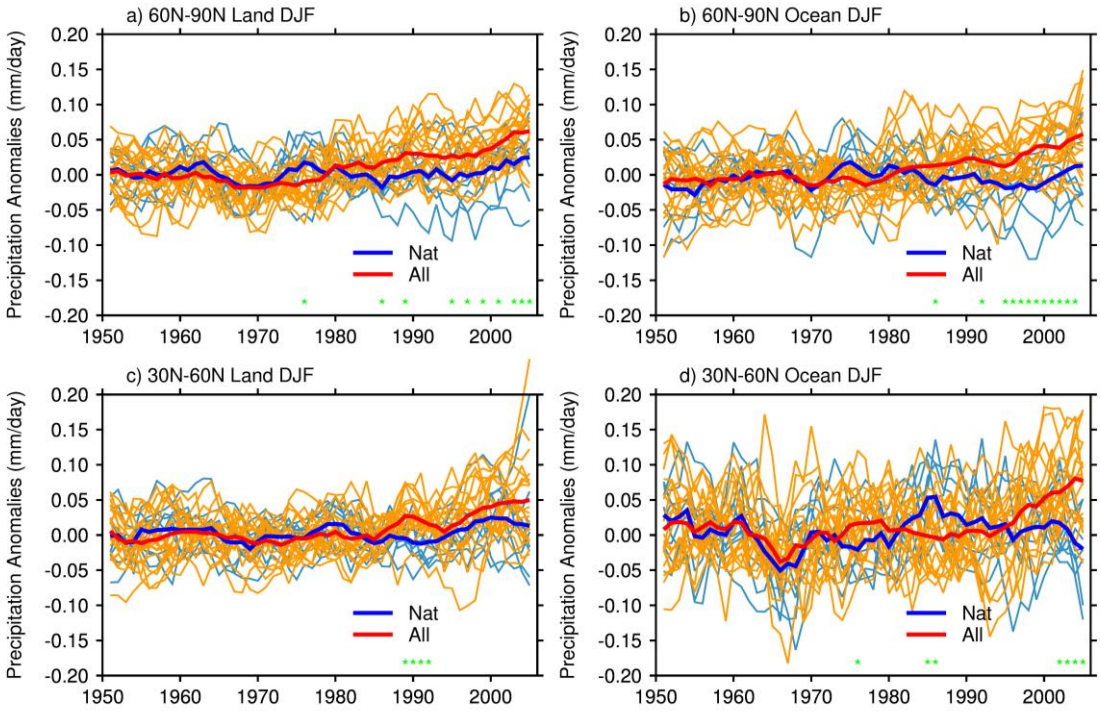

Figure 3: Zonal changes in DJF precipitation (mm/day), expressed relative to the baseline period of 1961-90, simulated by CMIP5 models forced with, both anthropogenic and natural forcings (ALL) and natural forcings only (NAT). a) 60^{o}N-90^{o}N Land , b) 60^{o}N-90^{o}N Ocean , c) 30^{o}N-60^{o}N Land, and d) 30^{o}N-60^{o}N Ocean, with all grid points. Blue lines show individual NAT simulations and red lines show individual ALL simulations specified in Table 1. Multi-model means are shown in thick solid lines. A 5-yr running mean is applied to the time series. Green stars show statistically significant changes at 5% level (p value < 0.05) between ALL and NAT runs using a two-sample two-tailed t-test for the last 30 years of the time series.

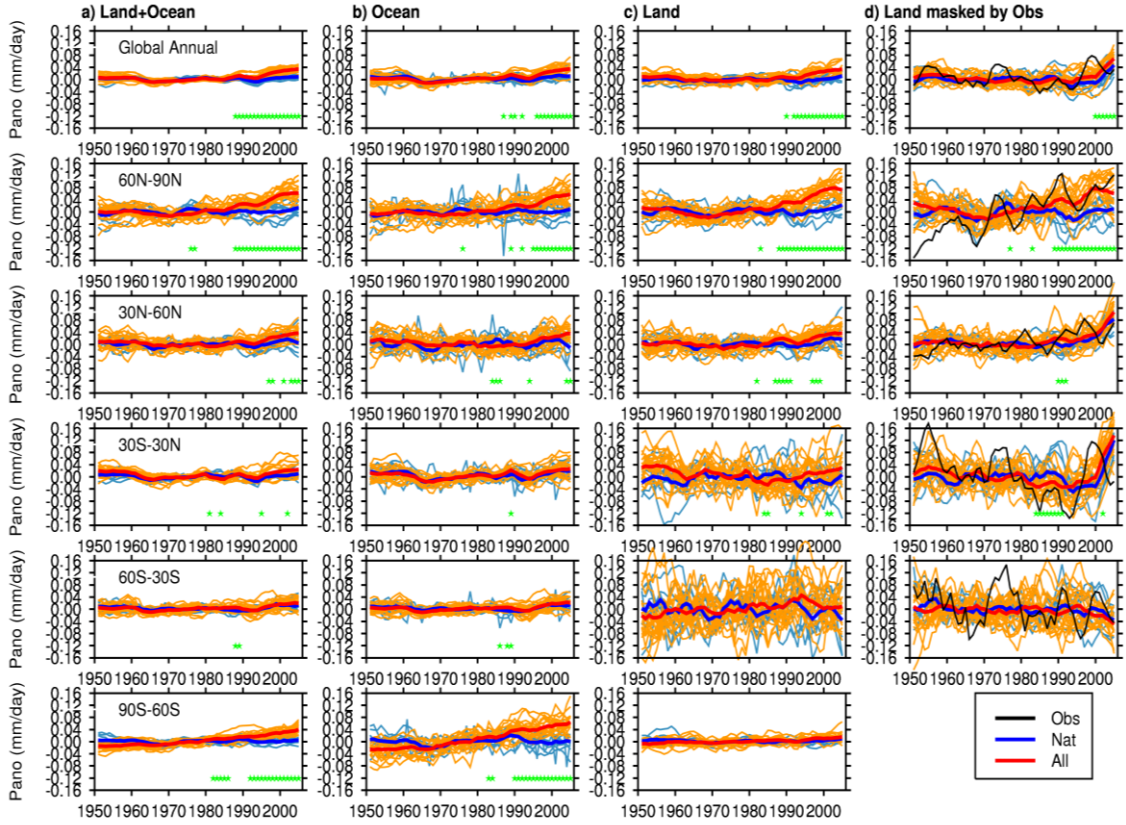

Supplementary Information Figure S1: Global and zonal changes in annual precipitation (mm/day), expressed relative to the baseline period of 1961-90, simulated by CMIP5 models forced with, both anthropogenic and natural forcings (ALL) and natural forcings only (NAT). a) Land and Ocean, b) Ocean , c) Land, with all grid points, and d) Land masked by observational coverage. Blue lines show individual NAT simulations and red lines show individual ALL simulations specified in Table 1. Multi-model means are shown in thick solid lines and observations are in black solid line. A 5-yr running mean is applied to both simulations and observations. Green stars show statistically significant changes at 5% level (p value < 0.05) between ALL and NAT runs using a two-sample two-tailed t-test for the last 30 years of the time series.

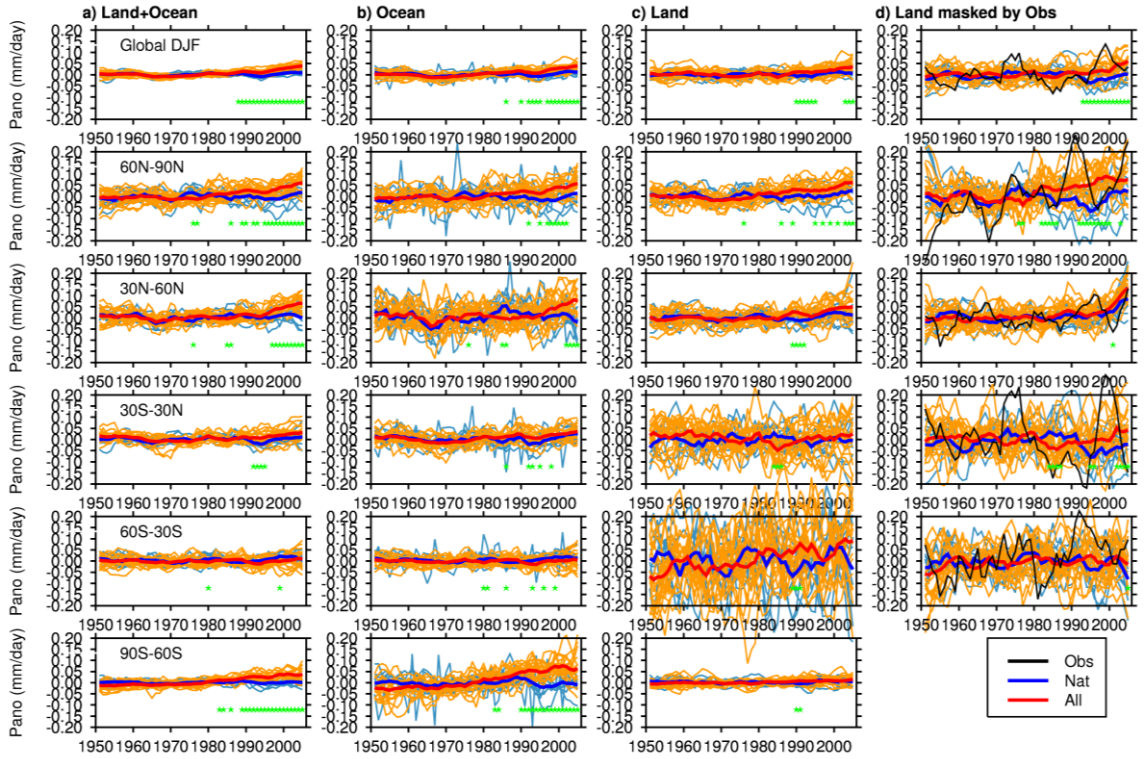

Supplementary Information Figure S2: Same as Figure S1, for DJF

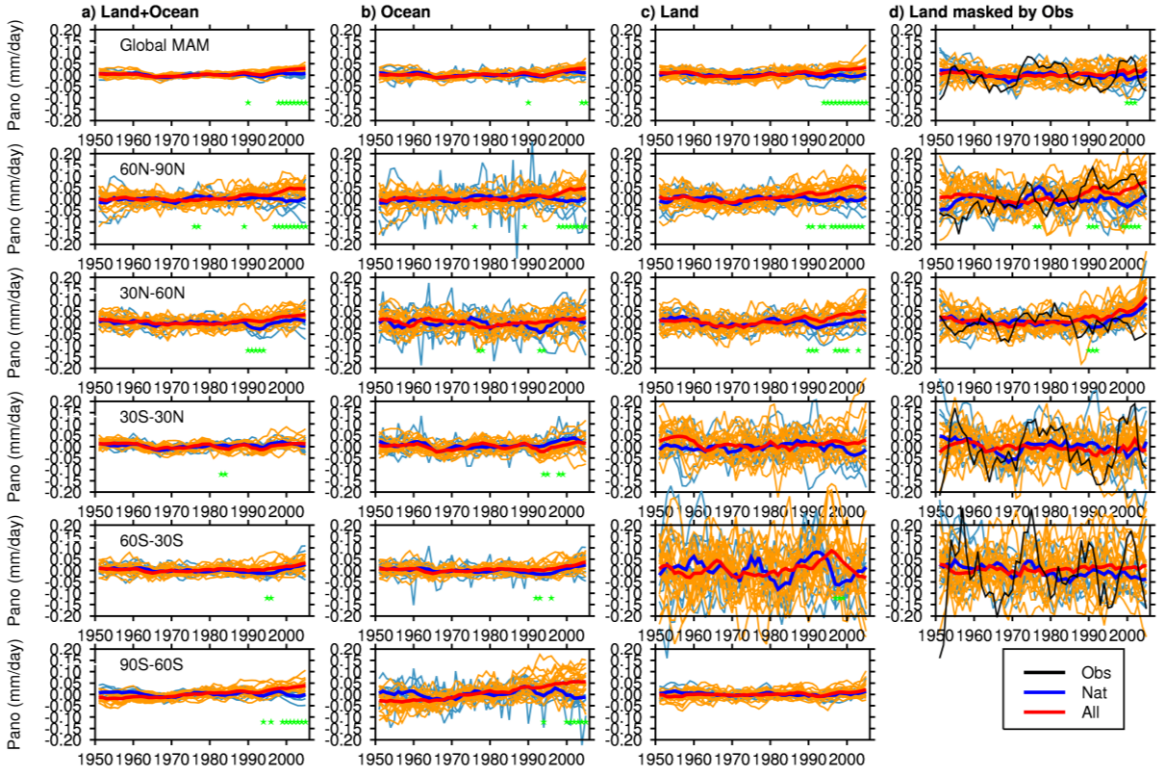

Supplementary Information Figure S3: Same as Figure S1, for MAM.

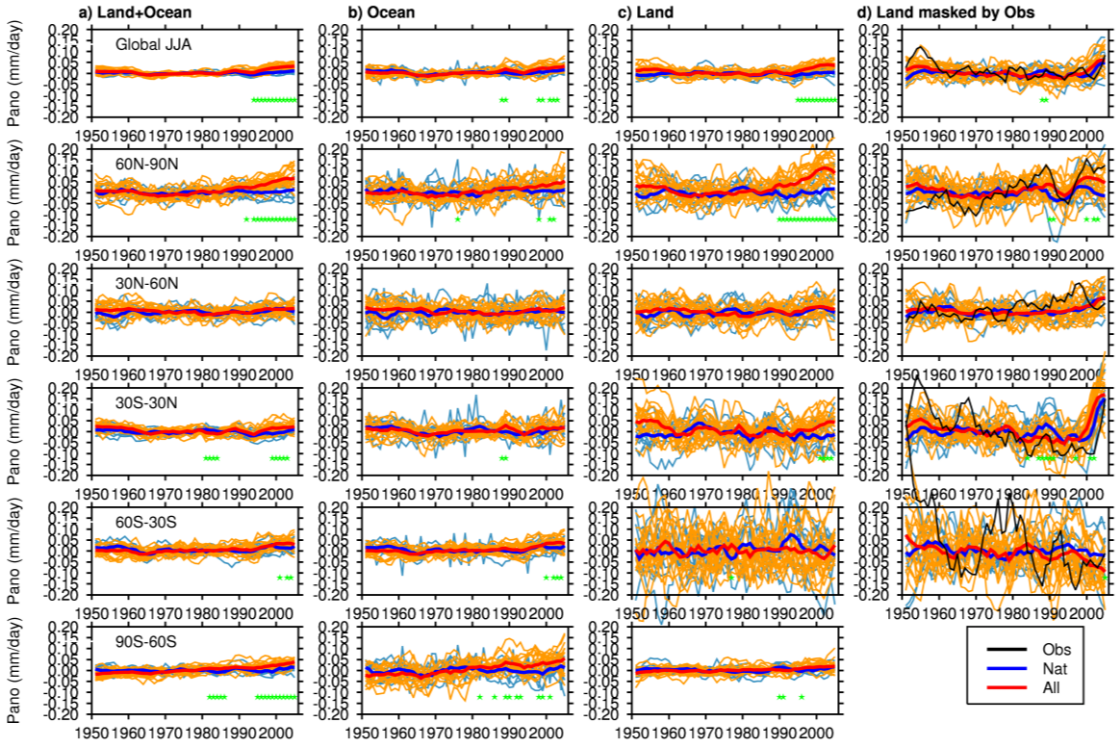

Supplementary Information Figure S4: Same as Figure S1, for JJA.

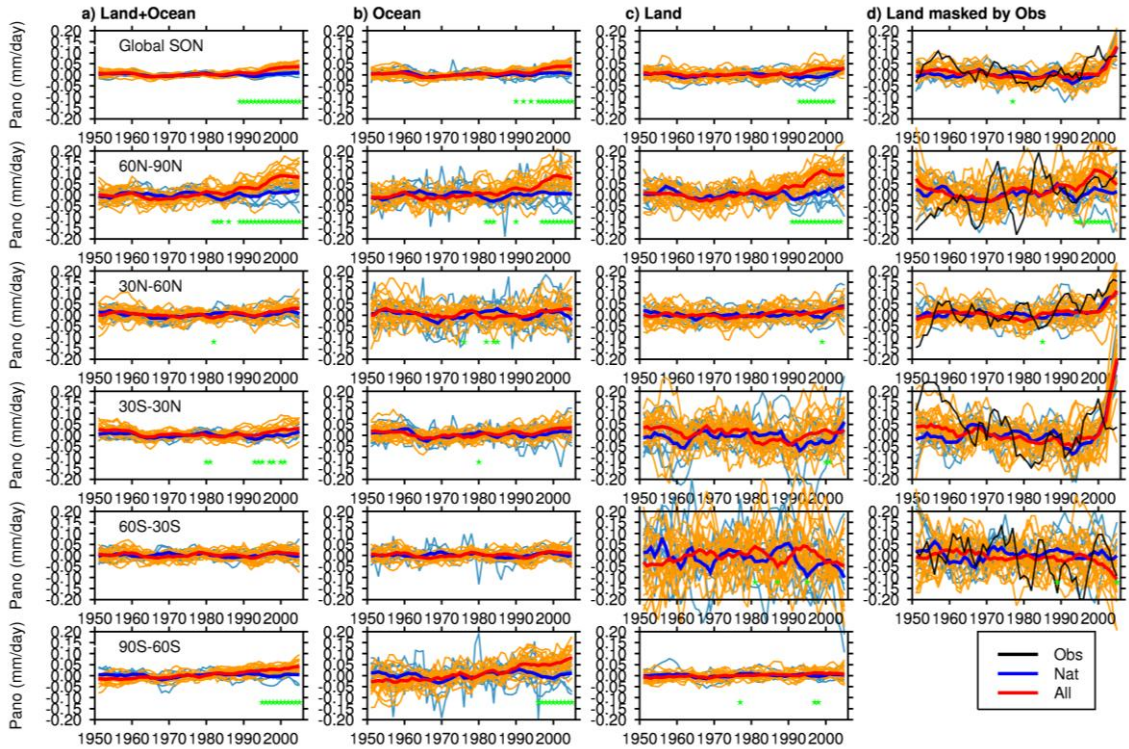

Supplementary Information Figure S5: Same as Figure S1, for SON.

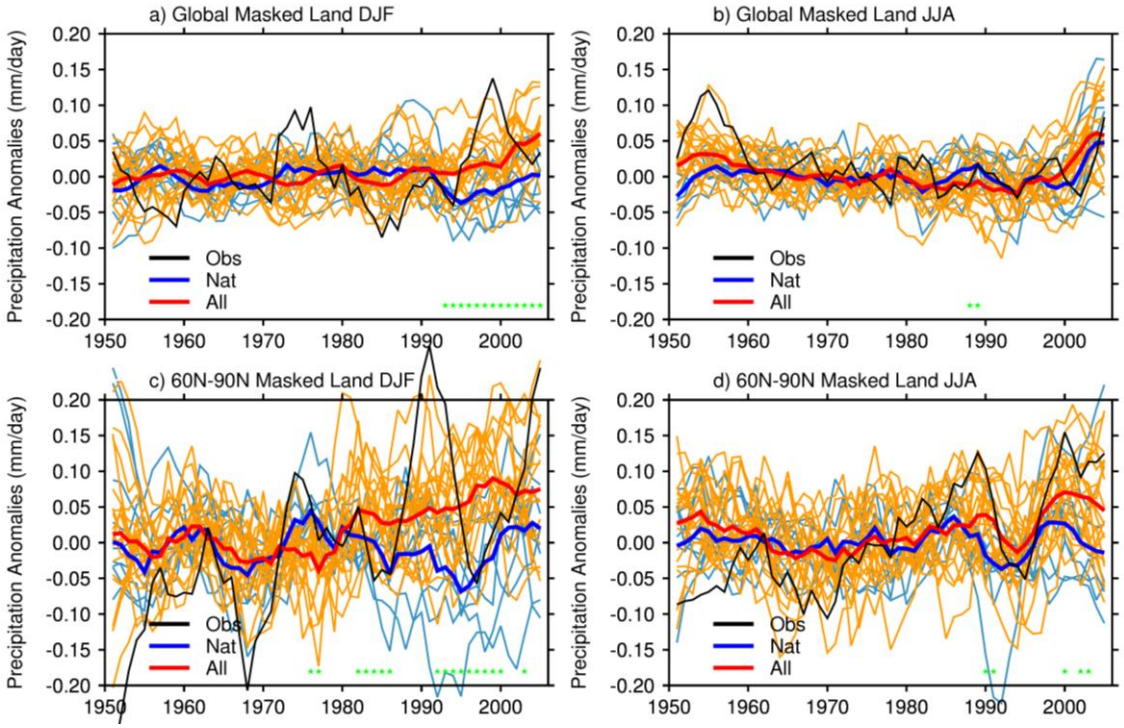

Figure S6: Global and zonal changes in seasonal precipitation (mm/day), expressed relative to the baseline period of 1961-90, simulated by CMIP5 models forced with, both anthropogenic and natural forcings (ALL) and natural forcings only (NAT). a) Global DJF Land , b) Global JJA Land , c) 60^{o}N-90^{o}N DJF Land, and d) 60^{o}N-90^{o}N JJA Land, masked by observational coverage. Blue lines show individual NAT simulations and red lines show individual ALL simulations specified in Table 1. Multi-model means are shown in thick solid lines and observations are in black solid line. A 5-yr running mean is applied to both simulations and observations. Green stars show statistically significant changes at 5% level (p value < 0.05) between ALL and NAT runs using a two-sample two-tailed t-test for the last 30 years of the time series.

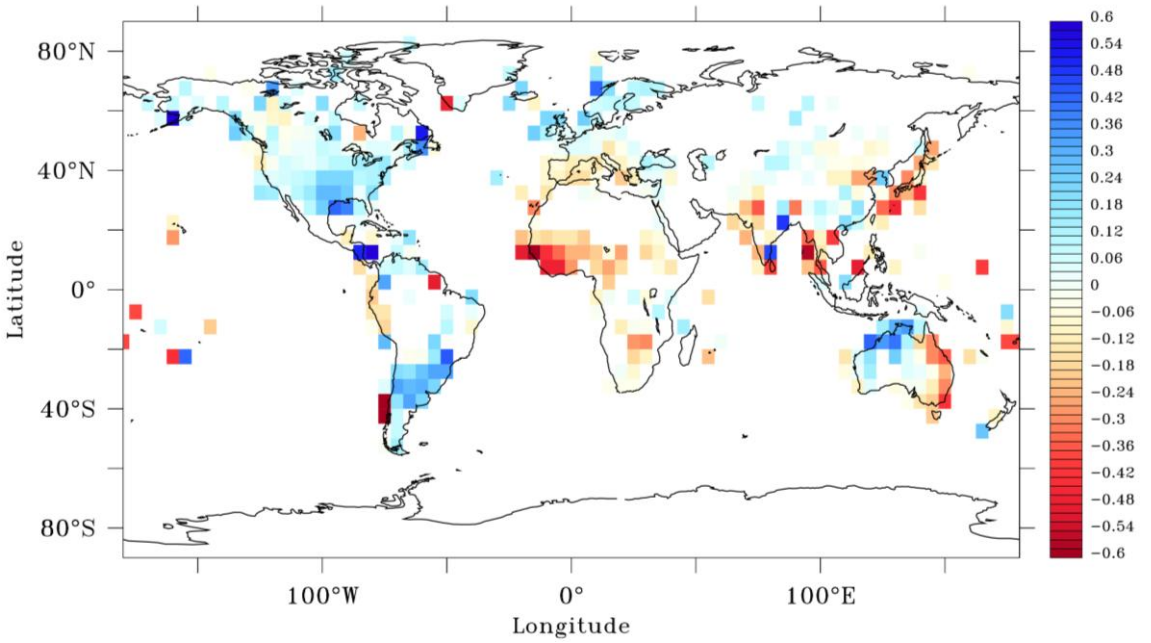

Figure S7: Spatial map of observed trend (mm/day/yr) using >75% of the observations of the total time period.

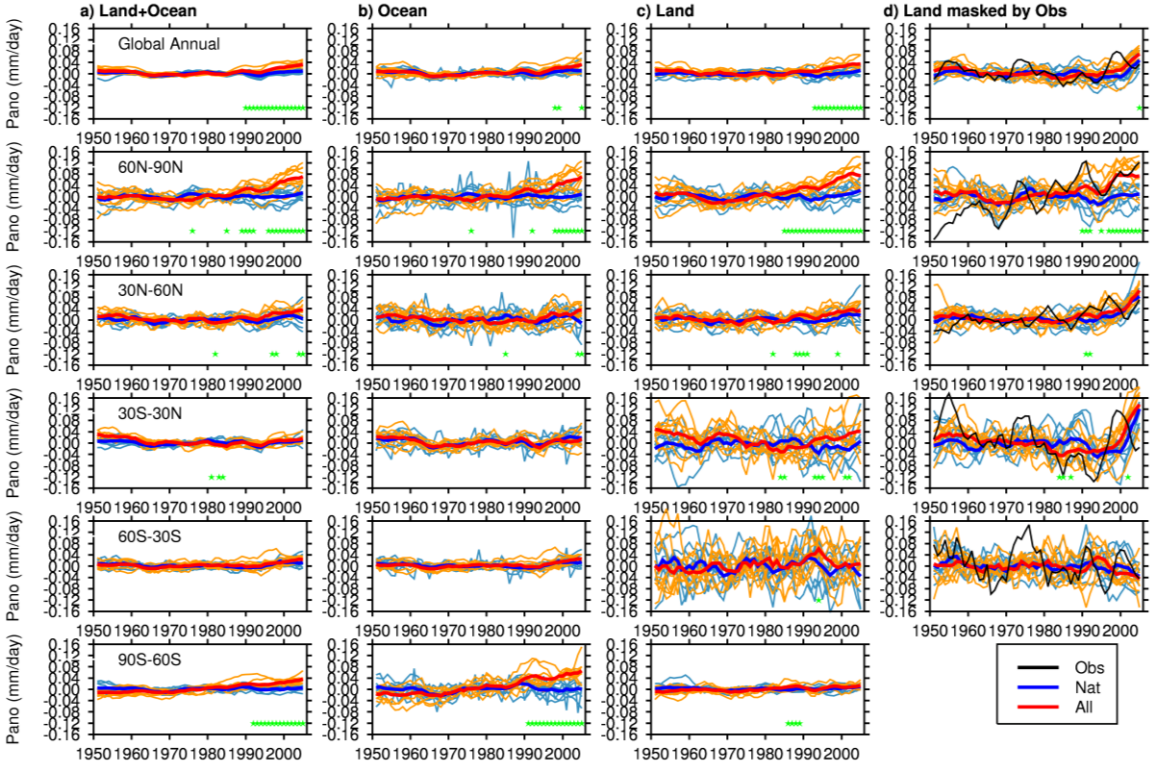

Figure S8: Same as Figure S1, but only ALL and NAT runs from identical models are plotted.